Published in final edited form as:
J Phys Chem C Nanomater Interfaces. 2013 May 23; 117(20): . doi:10.1021/jp402392y.

Surface-Enhanced Raman Spectroscopy of Polyelectrolyte-Wrapped Gold Nanoparticles in Colloidal Suspension

Sean T. Sivapalan[1,*], **Brent M. DeVetter**[2,3,*], **Timothy K. Yang**[4], **Matthew V. Schulmerich**[3,5], **Rohit Bhargava**[2,3,5,6], and **Catherine J. Murphy**[1,4]

[1]Department of Materials Science and Engineering, University of Illinois at Urbana-Champaign, Urbana, IL, 61801

[2]Department of Electrical and Computer Engineering, University of Illinois at Urbana-Champaign, Urbana, IL, 61801

[3]Beckman Institute for Advanced Science and Technology, University of Illinois at Urbana-Champaign, Urbana, IL, 61801

[4]Department of Chemistry, University of Illinois at Urbana-Champaign, Urbana, IL, 61801

[5]Department of Bioengineering, University of Illinois at Urbana-Champaign, Urbana, IL, 61801

[6]Department of Mechanical Science and Engineering, Micro and Nanotechnology Laboratory and University of Illinois Cancer Center, University of Illinois at Urbana-Champaign, Urbana, IL, 61801

Abstract

The rapidly expanding field of surface-enhanced Raman spectroscopy (SERS) has helped fuel an intense interest in noble metal nanoparticle synthesis. An in-suspension approach for quantifying SERS enhancement and relating that enhancement to a spontaneous Raman equivalent signal is described. Gold nanoparticles of various shapes were wrapped with polyelectrolyte multilayers that trapped Raman reporter molecules at defined distances from the metal core. Electrospray ionization liquid chromatography mass spectrometry (ESI-LC-MS) on digested samples was employed to measure the average number of bound Raman reporter molecules per gold nanoparticle, and inductively coupled plasma mass spectrometry (ICP-MS) was used to measure the average number of gold atoms per nanoparticle. Using these data, SERS signal intensity was compared to a spontaneous Raman calibration curve to compute a spontaneous Raman equivalent factor. Three different geometries of gold nanoparticles (cubes, spheres, and trisoctahedra) were synthesized to investigate edge and corner effects using these quantitative techniques. Finite element method (FEM) electromagnetic simulations examined the relationship between the different geometries and the observed SERS signal intensities. The experimental observations and theoretical results indicate that cubic gold nanoparticles have the highest effective signal.

Keywords

Surface enhanced Raman spectroscopy; gold nanoparticles; plasmonics; finite element method; SERS quantification

Corresponding authors: murphycj@illinois.edu (Catherine J. Murphy), rxb@illinois.edu (Rohit Bhargava).
*These authors contributed equally to this work.

Introduction

Plasmonic metal nanoparticles show great promise for biological applications, ranging from diagnostic imaging to *in vivo* therapies.[1–4] Intense electromagnetic fields near the metal surface, which arise from irradiation into the plasmon bands, promote highly sensitive surface-enhanced Raman scattering (SERS), both in substrate-based assays as well as nanoprobes approaching single molecule detection limits.[5] SERS has a dynamic range surpassing that of fluorescence spectroscopy[6] and the ability to multiplex vibrational fingerprints of reporter molecules.[4] The design considerations for such probes focus on maximizing the electromagnetic enhancement defined by their shape, size, and polarization of the incident light.[7] However, there has been great debate in the SERS community regarding the reproducibility and reliability of reported enhancement factors.[11]

Minor differences in synthesis and quantification approaches can produce varying results in the reported SERS enhancement. This is further complicated by sample preparation, such as whether or not the measurements were performed on dried colloidal suspensions, on SERS-active substrates, or on the colloidal suspensions themselves. In previous work we have demonstrated that gold nanocubes dried on gold substrates bearing an analyte monolayer have a higher SERS enhancement compared to gold nanorods prepared in the same way.[12] However, the structures that form as a result of nanoparticle drying have a complicated impact on the resulting signal; aggregation of nanoparticles can create electromagnetic hot-spots. Our understanding of these effects has rapidly accelerated due to the availability of computational tools based on the discrete dipole approximation (DDA), finite-difference time-domain (FDTD) method, and the finite element method (FEM), among others.[8–10] From simulations, it is well understood that hot-spots are localized areas of high enhancement resulting from interplasmonic coupling between metallic surfaces that may lead to unreliable or difficult-to-reproduce measurements.

In this study we aim to minimize the effects of hotspots by collecting SERS measurements on colloidal suspensions, and using polyelectrolyte-coated nanoparticles to reduce the effect of aggregation. Here, three different geometries (cubes, spheres, trisoctahedra) of gold nanoparticles were synthesized to investigate edge and corner effects. Raman-active reporter molecules trapped near the surface of gold nanoparticles were quantified using electrospray ionization liquid chromatography mass spectrometry (ESI-LC-MS). Additionally, the average number of gold atoms per nanoparticle were quantified via inductively coupled plasma mass spectrometry (ICP-MS). Using these data, we compare SERS signal intensity with a spontaneous Raman calibration curve. Finite element method (FEM) electromagnetic simulations were performed to examine the relationship between the different geometries and the observed SERS signal intensities.

Experimental Section

Materials

Hydrogen tetrachloride ($HAuCl_4$, > 99.999%), sodium borohydride ($NaBH_4$), polyallylamine hydrochloride (PAH, MW ≈ 15,000 g/mol), polyacrylic acid sodium salt (PAA, MW ≈ 15,000 g/mol, 35 wt. % in H_2O), sodium chloride (NaCl, > 99%), and ascorbic acid ($C_6H_8O_6$, > 99.0%) were obtained from Aldrich and used as received. Cetyltrimethylammonium bromide (CTAB, > 99%) and cetyltrimethylammonium chloride (CTAC, > 98%) were obtained from Sigma and used without further purification. All glassware were cleaned using aqua regia and rinsed with Barnstead E-Pure 18 MI-cm water.

Instrumentation

SERS spectra were obtained on a Horiba LabRAM Raman microscope configured with a 785 nm excitation laser line. Triplicate measurements with integration times of 30 seconds were performed on the gold nanoparticles in suspension through a 1 cm path length quartz cuvette. Laser power at the sample was measured to be 12.5 mW. Zeta potential measurements were performed on a Brookhaven ZetaPALS instrument. Electronic absorption spectra were measured with a Cary 500 scan UV-Vis-NIR spectrophotometer. Transmission electron micrograph (TEM) images were taken on a JEOL 2010F Field Emission Microscope at 200 kV accelerating voltage. For grid preparation 10 μL of gold nanoparticle suspension was drop cast onto holey carbon TEM grids (Pacific Grid-Tech). Size distributions were verified by analyzing at least 100 representative particles per shape. We use a Thermo Scientific Sorvall Legend X1 Centrifuge for purification as detailed in the synthesis below.

Synthesis of seeds for CTAB cubes (A)

The nanoparticle seeds were synthesized by modification the method of El-Sayed et al.[13] An aqueous CTAB solution (7.5 mL, 0.1 M) was mixed with 0.25 mL of 0.01 M aqueous $HAuCl_4$. To the stirred solution, 0.6 mL of ice-cold newly-made aqueous 0.01 M $NaBH_4$ was quickly added, which resulted in a light brown solution. After stirring the solution vigorously for 2 minutes, the solution was kept for 1 hour in room temperature before use.

Synthesis of CTAB seeds for trisoctahedra (TOH) gold nanocrystals (B)

The nanoparticle seeds were synthesized by following the procedure by El-Sayed et al.[13] An aqueous CTAB solution (7.0 mL, 75 mM) was mixed with 46 μL of 20 mM aqueous $HAuCl_4$. To the solution, 0.42 mL of ice-cold freshly made aqueous 0.01 M $NaBH_4$ was quickly added under vigorous mixing yielding a light brown solution. After $NaBH_4$ was added, the solution was gently stirred to decompose the excess $NaBH_4$. The solution was used within 2–5 hours after preparation.

Synthesis of CTAB spheres and cubes

Spheres and cubes were synthesized in 40 mL batches. To 32 mL of nanopure water, aqueous solutions of 6.4 mL of 0.1 M CTAB and 0.8 mL of 0.01 M $HAuCl_4$ were added, respectively. This resulted in a yellow-brown solution. Then, 3.8 mL of aqueous 0.1 M ascorbic acid was added as the reducing agent, which rendered the solution colorless. From here depending on the seed concentration, spheres or cubes will form. To obtain spheres, a 0.02 mL of 5 times diluted seed (A) was added to the colorless solution. To obtain cubes, 0.03 mL of 10 times diluted seed (A) was added to the colorless solution. Solutions were allowed to react until no further color changes were observed. The spheres were centrifuged at 4000 rcf for 30 minutes and the supernatant was removed. The pellet was re-suspended in water and this process was repeated again to remove excess CTAB. Similarly, cubes were twice centrifuged at 8000 rpm for 20 minutes.

Synthesis of TOH gold nanocrystals

Trisoctahedra (TOH) nanocrystals were synthesized by a seed mediated method used by Lee et al.[14] A 0.125 mL solution of aqueous 20 mM $HAuCl_4$ was mixed with 9 mL of 22 mM aqueous CTAC. To this mixture, 3.06 mL of aqueous 38.8 mM ascorbic acid was added to make the concentration of ascorbic acid 9.5 mM. The solution was thoroughly mixed. Then, seed (B) was diluted 100 fold with nanopure water, and 50 μL of the diluted seed (B) was added to the solution. This resulted in a red-pinkish solution. Trisoctahedra samples were purified by centrifugation at 4000 rcf for 30 minutes. The supernatant was discarded and the

sample was re-suspended in water. To remove excess CTAC, this process was repeated twice.

Polyelectrolyte wrapping and complexation of methylene blue to gold nanoparticles

To 30 mL of as synthesized CTAB/CTAC stabilized gold nanoparticles, 6 mL of PAA (10 mg/mL) and 3 mL of NaCl (10 mM) were added and left overnight. Centrifugation and re-suspension into 30 mL of water was performed on each sample to remove excess PAA at the same speeds specified in the synthesis for each shape. To complex the gold nanoparticles with Raman reporter, 1 mL of methylene blue (1 mM) was added to the suspension. After 1 hour, centrifugation was performed again to remove unbound methylene blue. To 30 mL of re-suspended gold nanoparticles, 6 mL of PAH (10 mg/mL) and 3 mL of NaCl (10 mM) was added and left overnight. The samples were again centrifuged to remove excess PAH. Dialysis with 20,000 g/mol dialysis cassettes (Fischer Scientific) was performed for 48 hours in 4 L of water to remove residual reagents. To quantify the number of methylene blue molecules via liquid chromatography mass spectrometry, 1 mL of methylene blue complexed polyelectrolyte wrapped gold nanoparticles were centrifuged into pellets and re-suspended into 50 μL of water. To this suspension, 10 μL of 1 M KCN was added and allowed to sit for at least 1 hour before quantification. The suspension slowly turned colorless as the gold nanoparticles were etched away.

ESI-LC-MS quantification of methylene blue

The LC-MS analysis was performed in Metabolomics Center at UIUC with a 5500 QTRAP mass spectrometer (AB Sciex, Foster City, CA) which is equipped with a 1200 Agilent LC. Analyst (version 1.5.1, Applied Biosytems) was used for data acquisition and processing. An Agilent Zorbax SB-Aq column (5u, 50 × 4.6 mm) was used for the separation. The HPLC flow rate was set at 0.3 mL/min. HPLC mobile phases consisted of A (0.1% formic acid in H_2O) and B (0.1% formic acid in acetonitrile). The gradient was: 0–1 min, 98% A; 6–10 min, 2% A; 10.5–17 min, 98% A. The autosampler was kept at 5°C. The injection volume was 1 μL. The mass spectrometer was operated with positive electrospray ionization. The electrospray voltage was set to 2500 V, the heater was set at 400°C, the curtain gas was 35, and GS1 and GS2 were 50, 55, respectively. Quantitative analysis was performed via multiple reaction monitoring (MRM) where m/z 284.2 to m/z 240.1 was monitored.

Results and Discussion

Polyelectrolyte-wrapped nanoparticles are highly resistant to aggregation and provide a buffering layer of roughly 5 nm from each metallic surface.[15] Raman-active molecules of methylene blue were electrostatically trapped between a layer of anionic polyacrylic acid (PAA) and cationic polyallylamine hydrochloride (PAH). Three nanoparticle geometries (cubes, spheres, and trisoctahedra) with polyelectrolyte layers and trapped methylene blue molecules are depicted in Figure 1 with their corresponding transmission electron micrograph (TEM) images. Each synthetic step was verified using zeta potential measurements to indicate successful wrapping.

The far-field optical properties of the colloidal suspensions are nearly identical as shown in the experimental electronic absorption spectra (Figure 2). Recently, we have demonstrated a dependence on realized signal for in-suspension measurements due to an interrelationship between localized surface plasmon resonance (LSPR) and laser excitation wavelength.[16] Nanoparticle suspensions were synthesized with similar LSPR maxima in order minimize these effects. Here, four independently synthesized batches of cubes, spheres, and trisoctahedra had LSPR maxima at 543 nm, 537 nm, and 529 nm, respectively, to maximize

signal for 785 nm excitation.[16] Characterization with TEM revealed the average size of each shape to be 54.3 ± 3.35 nm, 46.54 ± 6.7 nm, and 52.3 ± 5.8 nm for cubes, spheres, and trisoctahedra, respectively. The average number of reporter molecules (methylene blue) per nanoparticle shape were quantified with ESI-LC-MS against known concentrations of reporter standards (see Experimental Section). On average, there were between 1200 and 2400 molecules per gold nanoparticle. Both experimental[17] and theoretical[18] reports typically assume monolayer coverage of Raman-active molecules. With an assumed molecular profile of 0.66 nm^2/molecule for methylene blue,[19] expected monolayer coverage was over 10,000 molecules per nanoparticle. In all cases, each nanoparticle shape had less than 25% coverage (Figure (2(d)).

Quantitative comparison of SERS data were performed by measuring the spontaneous Raman intensity of methylene blue in water with 25 μM – 400 μM concentrations. All measurements were acquired with exactly the same laser power, acquisition times, and laser configuration used for SERS measurements. From these data, a spontaneous Raman calibration curve was constructed via integration of the band at ~1625 cm^{-1} (Figure 3). Due to conformational changes in the methylene blue molecules during the binding process, SERS signal intensity was quantified at 1616 cm^{-1}. SERS measurements were performed in aqueous solution on nanoparticle ensembles at an average concentration of 0.074 nM, 0.12 nM, and 0.17 nM for cubes, spheres, and trisoctahedra, respectively.

An observed Raman intensity (Table 1) may be calculated from extrapolation of the spontaneous Raman calibration curve such that:

$$\text{Observed Raman Intensity} = \frac{(\text{SERS}_{1616} - 12472)}{157\, N_{\text{conc}} M_{\text{molec}}}$$

where N_{conc} is the average concentration of gold nanoparticles and M_{molec} is the average number of reporter molecules per nanoparticle. The slope m = 157 and the y-intercept b = 12472 were determined from linear regression of the spontaneous calibration curve. The indicated error corresponds to the averaged standard deviation of reporter molecules per sample as determined by ESI-LC-MS. Gold nanocubes have the highest observed intensity of 5.63×10^3.

Nanostructures with high radii of curvature concentrate optical fields through the so-called “lightning rod” effect of SERS.[20] Recent computational studies have emphasized the importance of edge effects in SERS-based measurements.[21, 22] We performed FEM electromagnetic simulations to visualize edge effects on nonspherical geometries. In contrast to other popular techniques such as FDTD and DDA, FEM utilizes adaptive meshes rather than cubic grids subsequently improving near-field accuracy as well as significantly decreasing solver time.[18] All calculations were performed using a commercial software package (COMSOL Multiphysics 4.2). Bulk gold optical constants were obtained from Johnson and Christy.[23]

Cubes, spheres, and trisoctahedra were simulated in a three-dimensional scattering domain. Electromagnetic enhancement is quantified by a factor G where it is assumed that the Stokes’ shifted wavelength of Raman scattered light is negligible: $G = |E(\lambda_{inc})|^2 \, |E(\lambda_{inc} + \delta\lambda)|^2 \approx |E(\lambda_{inc})|^4$. Assuming submersion in water (n = 1.33), cubes were modeled with an edge length of 54 nm, spheres with a diameter of 46 nm, and trisoctahedra with an effective diameter of 52 nm, corresponding to the average dimensions measured in TEM. The polyelectrolyte layers were not included in the simulation. Furthermore, we neglect any chemical enhancement effects, as they are expected to be minimal with our chosen reporter molecule. Corner roundness was empirically determined from TEM image analysis using ImageJ software developed at the National Institutes of Health (Figure 1). As expected from the lightning rod effect, nanostructures with the sharpest corners have the highest

enhancement factor G. Despite having more corners, trisoctahedra are relatively smooth as compared to the edges of gold nanocubes.

Surface integration of $|E|^4$ normalized to nanoparticle surface area reveal cubes have a 2.5× greater field strength as compared to trisoctahedra and spheres. The observed Raman intensity, however, of cubes is over 5x greater than that of spheres. Trisoctahedra have an observed intensity greater than 4x that of spheres. Therefore, we suggest that the primary mechanism of enhancement is due to the lightning rod effect because of the sharp edges and corners that exist on the cubes and trisoctahedra. Differences in the simulated versus experimental data arise from variability in the molecular trap coating process. In the absence of definitive imaging results, we propose that the polyelectrolyte coating process uniformly deposits over the entire surface of each nanoparticle shape. However, molecules positioned at corners or edges may be displaced farther from the surface than molecules trapped near smooth features. Mismatch between theory and experiment is likely due to the difficulties in determining the positions of reporter molecules.

The quantitative approach to ensemble SERS measurements presented here demonstrates a novel method to compute observed Raman intensity using a spontaneous Raman calibration curve. In combination with reporter molecule and gold nanoparticle quantification, we have demonstrated that gold nanocubes have the highest SERS signal relative to trisoctahedra and spheres. Trisoctahedra bearing high-index facets such as (221), (331) and (441)[24] are of particular interest due to their increased chemical reactivity.[25] Future work will involve studying the binding density and binding sites available to SERS-active molecules on high-index nanostructures.

Acknowledgments

STS and BMD acknowledge support from the University of Illinois at Urbana-Champaign from NIH National Cancer Institute Alliance for Nanotechnology in Cancer ‘Midwest Cancer Nanotechnology Training Center’ Grant R25 CA154015A. MVS acknowledges support through the Congressionally Directed Medical Research Program Postdoctoral Fellowship BC101112. We also acknowledge support from a Beckman Institute seed grant, AFOSR Grant Number FA 9550-09-1-0246 and NSF Grant Numbers CHE-1011980 and CHE 0957849. The authors thank the Roy J. Carver Biotechnology Metabolomics Center at the University of Illinois at Urbana-Champaign for mass spectrometry analysis. TEM images were obtained at the Frederick Seitz Materials Research Laboratory Central Facilities, University of Illinois.

References

1. Boisselier E, Astruc D. Gold Nanoparticles in Nanomedicine: Preparations, Imaging, Diagnostics, Therapies and Toxicity. Chem Soc Rev. 2009; 38:1759–1782. [PubMed: 19587967]
2. Qian XM, Peng XH, Ansari DO, Yin-Goen Q, Chen GZ, Shin DM, Yang L, Young AN, Wang MD, Nie SM. In Vivo Tumor Targeting and Spectroscopic Detection with Surface-Enhanced Raman Nanoparticle Tags. Nature Biotechnol. 2008; 26:83–90. [PubMed: 18157119]
3. von Maltzahn G, Park JH, Agrawal A, Bandaru NK, Das SK, Sailor MJ, Bhatia SN. Computationally Guided Photothermal Tumor Therapy Using Long-Circulating Gold Nanorod Antennas. Cancer Res. 2009; 69:3892–3900. [PubMed: 19366797]
4. Zavaleta CL, Smith BR, Walton I, Doering W, Davis G, Shojaei B, Natan MJ, Gambhir SS. Multiplexed Imaging of Surface Enhanced Raman Scattering Nanotags in Living Mice Using Noninvasive Raman Spectroscopy. Proc Natl Acad Sc USA. 2009; 106:13511–13516. [PubMed: 19666578]
5. Nie SM, Emory SR. Probing Single Molecules and Single Nanoparticles by Surface-Enhanced Raman Scattering. Science. 1997; 275:1102–1106. [PubMed: 9027306]
6. Pieczonka NPW, Aroca RF. Single Molecule Analysis by Surfaced-Enhanced Raman Scattering. Chem Soc Rev. 2008; 37:946–954. [PubMed: 18443680]

7. Alvarez-Puebla RA. Effects of the Excitation Wavelength on the SERS Spectrum. J Phys Chem Lett. 2012; 3:857–866.
8. Atkinson, AL.; McMahon, JM.; Schatz, GC. FDTD Studies of Metallic Nanoparticle Systems - Self Organization of Molecular Systems. Russo, N.; Antonchenko, VY.; Kryachko, ES., editors. Springer; Netherlands: 2009. p. 11-32.
9. Jain PK, Lee KS, El-Sayed IH, El-Sayed MA. Calculated Absorption and Scattering Properties of Gold Nanoparticles of Different Size, Shape, and Composition: Applications in Bioloigcal Imaging and Biomedicine. J Phys Chem B. 2006; 110:7238–7248. [PubMed: 16599493]
10. Khoury CG, Norton SJ, Vo-Dinh T. Plasmonics of 3-D Nanoshell Dimers Using Multipole Expansion and Finite Element Method. ACS Nano. 2009; 3:2776–2788. [PubMed: 19678677]
11. Margueritat J, Gehan H, Grand J, Lévi G, Aubard J, Félidj N, Bouhelier A, Colas-Des-Francs G, Markey L, Marco De Lucas C, et al. Influence of the Number of Nanoparticles on the Enhancement Properties of Surface-Enhanced Raman Scattering Active Area: Sensitivity Versus Repeatability. ACS Nano. 2011; 5:1630–1638. [PubMed: 21366249]
12. Orendorff CJ, Gole A, Sau TK, Murphy CJ. Surface-Enhanced Raman Spectroscopy of Self-Assembled Monolayers: Sandwich Architecture and Nanoparticle Shape Dependence. Anal Chem. 2005; 77:3261–3266. [PubMed: 15889917]
13. Nikoobakht B, El-Sayed MA. Preparation and Growth Mechanism of Gold Nanorods (NRs) Using Seed-Mediated Growth Method. Chem Mater. 2003; 15:1957–1962.
14. Yu Y, Zhang QB, Lu XM, Lee JY. Seed-Mediated Synthesis of Monodisperse Concave Trisoctahedral Gold Nanocrystals with Controllable Sizes. J Phys Chem C. 2010; 114:11119–11126.
15. Gole A, Murphy CJ. Polyelectrolyte-Coated Gold Nanorods: Synthesis, Characterization and Immobilization. Chem Mater. 2005; 17:1325–1330.
16. Sivapalan ST, DeVetter BM, Yang TK, van Dijk T, Schulmerich MV, Carney PS, Bhargava R, Murphy CJ. Off-resonance Surface-Enhanced Raman Spectroscopy from Gold Nanorod Suspensions as a Function of Aspect Ratio: Not What We Thought. ACS Nano. 2013 in press.
17. Naujok RR, Duevel RV, Corn RM. Fluorescence and Fourier-Transform Surface-Enhanced Raman-Scattering Measurements of Methylene-Blue Adsorbed onto a Sulfur-Modified Gold Electrode. Langmuir. 1993; 9:1771–1774.
18. Kerker M, Wang DS, Chew H. Surface Enhanced Raman-Scattering (SERS) by Molecules Adsorbed at Spherical Particles. Appl Optic. 1980; 19:4159–4174.
19. Hahner G, Marti A, Spencer ND, Caseri WR. Orientation and Electronic Structure of Methylene Blue on Mica: A Near Edge X-ray Absorption Fine Structure Spectroscopy Study. J Chem Phys. 1996; 104:7749–7757.
20. Liao PF, Wokaun A. Lightning Rod Effect in Surface Enhanced Raman Scattering. The Journal of Chemical Physics. 1982; 76:751–752.
21. Angulo AM, Noguez C, Schatz GC. Electromagnetic Field Enhancement for Wedge-Shaped Metal Nanostructures. J Phys Chem Lett. 2011; 2:1978–1983.
22. Xu H, Aizpurua J, Käll M, Apell P. Electromagnetic Contributions to Single-molecule Sensitivity in Surface-enhanced Raman Scattering. Phys Rev E. 2000; 62:4318–4324.
23. Johnson PB, Christy RW. Optical Constants of Noble Metals. Phys Rev B. 1972; 6:4370–4379.
24. Ma Y, Kuang Q, Jiang Z, Xie Z, Huang R, Zheng L. Synthesis of Trisoctahedral Gold Nanocrystals with Exposed High-Index Facets by a Facile Chemical Method. Angew Chem Int Edit. 2008; 47:8901–8904.
25. Zhang J, Langilee MR, Personick ML, Zhang K, Li S, Mirkin CA. Concave Cubic Gold Nanocrystals with High-Index Facets. J Am Chem Soc. 2010; 132:14012–14014. [PubMed: 20853848]

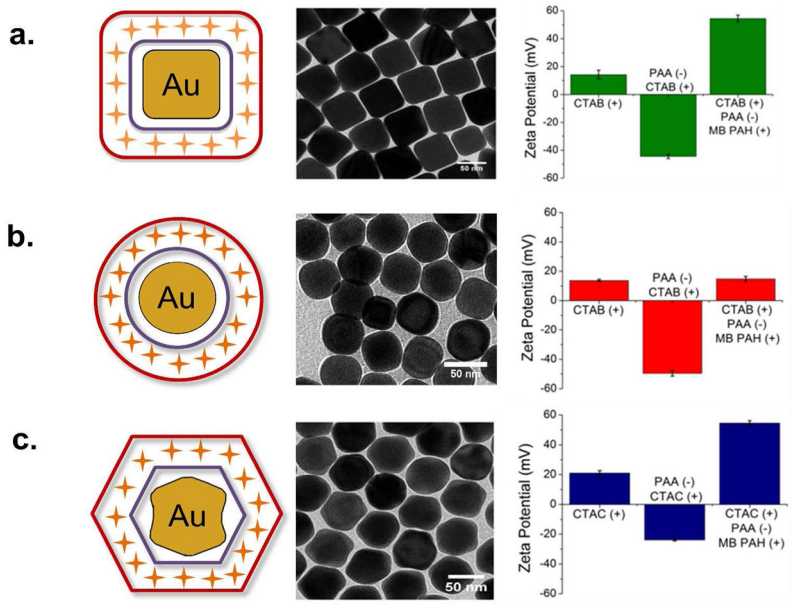

Figure 1.

Cartoon illustrating polyelectrolyte trap coating of methylene blue (MB, orange crosses) around gold nanoparticles. MB is electrostatically bound to polyacrylic acid (PAA, purple) and trapped by polyallylamine hydrochloride (PAH, dark red). Transmission electron micrographs of nanoparticle shapes and corresponding zeta potential for (a) cubes (b) spheres and (c) trisoctahedra as a function of wrapping stage.

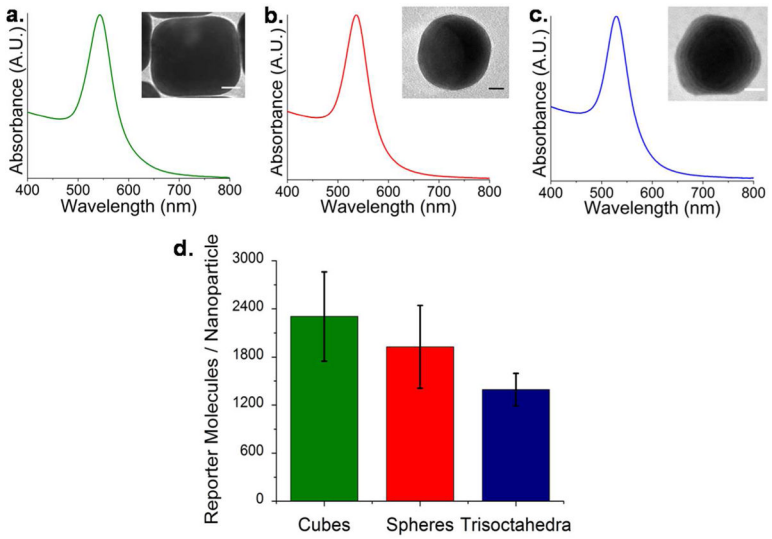

Figure 2.

Normalized electronic absorption spectra of colloidal suspensions of (a) cubes, (b) spheres, and (c) trisoctahedra. Inset: transmission electron micrographs of each shape. Scale bars = 10 nm. (d) Experimental ESI-LC-MS quantification of the average number of methylene blue molecules per gold nanoparticle shape. Error bars indicate the standard deviation over four independently synthesized samples.

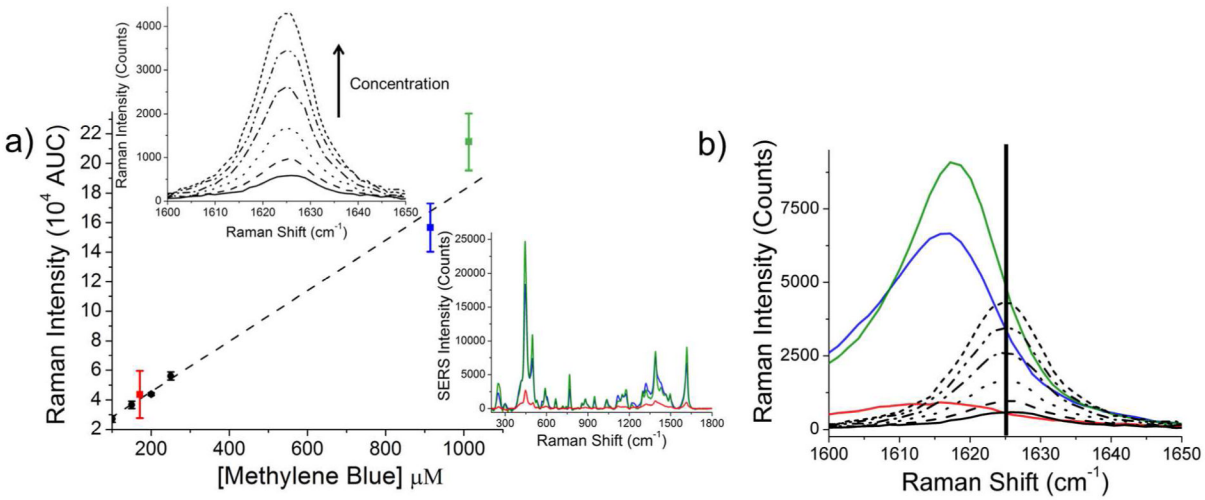

Figure 3.

(a) Spontaneous Raman calibration curve of the ~1625 cm^{-1} band of methylene blue (black dots), compared to the same concentration of methylene blue bound to gold nanospheres (red square), gold trisoctahedra (blue square) and gold nanocubes (green square). Error bars correspond to the standard deviation of nanoparticle concentration and reporter molecules per nanoparticle as determined by ICP-MS and ESI-LC-MS, respectively. Top left inset: Spontaneous Raman spectra (between 1600 cm^{-1} and 1650 cm^{-1}) of varying concentrations of methylene blue in water (25 – 400 μM). Bottom right inset: Example spectra calculated from the spontaneous Raman calibration curve with an assumed 0.12 nM gold nanoparticle concentration and 1800 reporter molecules per nanoparticle. (b) Methylene blue molecules experience a conformational change during the trap-coating process, resulting in a slight shift in the observed Raman band. Raman measurements of free methylene blue molecules (vertical bar at 1625 cm^{-1}) versus surface-enhanced trap-coated methylene blue molecules are shown (cubes, green; trisoctahedra, blue; spheres, red).

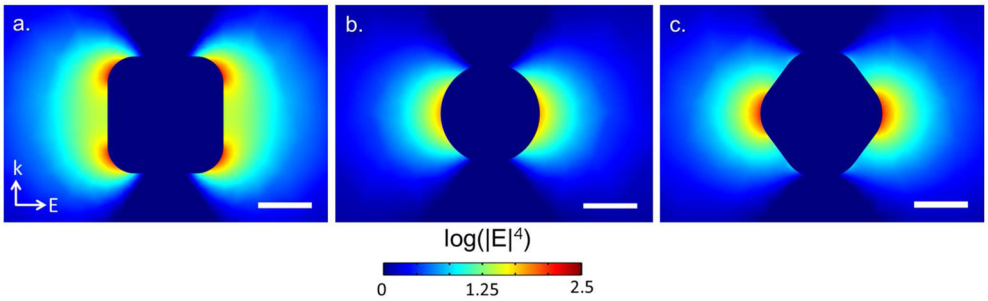

Figure 4.
Electric field distributions of single nanoparticle shapes (a) 54 nm diameter cube (b) 46 nm diameter sphere (c) 52 nm diameter trisoctahedra evaluated at λ = 785 nm. Water (n = 1.33) is assumed to be the surrounding media. Scale bar 25 nm.

Table 1

Observed Raman intensity of each nanoparticle shape. Intensity values were determined from extrapolation of the spontaneous Raman calibration curve of methylene blue with SERS measurements normalized to nanoparticle concentration (determined by ICP-MS) and the average number of reporter molecules per nanoparticle (determined by ESI-LC-MS).

Nanoparticle Shape	Observed Raman Intensity
Cubes	$5.63 \pm 0.56 \times 10^3$
Spheres	$0.87 \pm 0.52 \times 10^3$
Trisoctahedra	$4.01 \pm 0.20 \times 10^3$